THE ASTROPHYSICAL JOURNAL, 411:L41–L44, 1993 July 1


# CORONAGRAPHIC IMAGING OF THE β PICTORIS CIRCUMSTELLAR DISK: EVIDENCE OF CHANGING DISK STRUCTURE WITHIN 100 AU[1]

DAVID A. GOLIMOWSKI AND SAMUEL T. DURRANCE
Center for Astrophysical Sciences, Department of Physics and Astronomy, The Johns Hopkins University, Baltimore, MD 21218
AND
MARK CLAMPIN
Space Telescope Science Institute, 3700 San Martin Drive, Baltimore, MD 21218
*Received 1993 February 26; accepted 1993 April 16*

## ABSTRACT

New *R*-band images of the β Pictoris circumstellar disk obtained with the Adaptive Optics Coronagraph expose the disk inward to 40 AU from the star. From these images, the first reliable optical photometry of the disk within 100 AU of β Pic is reported. Across a radius of 100 AU, the radial power-law dependence of the disk-midplane surface brightness undergoes an abrupt transition, with power-law indices changing within 100 AU from −3.5 to −2.4 in the NE extension and from −4.2 to −1.9 in the SW extension. This result confirms the previously noted asymmetry in the brightness gradient beyond 250 AU, and suggests an inverted asymmetry within 100 AU. The geometrical thickness of the disk appears nearly constant within ∼115 AU and increases proportionally with radius beyond ∼115 AU. These changes in brightness gradient and disk thickness are consistent with the two-component disk models of Backman et al. The observed changes in disk structure at ∼100 AU may mark the boundary of rapid ice sublimation within which only refractory grains exist, but may also reflect a flattened grain distribution associated with planetary formation within 40 AU.

*Subject headings:* stars: circumstellar matter — stars: individual (β Pictoris)

## 1. INTRODUCTION

The A5V star β Pictoris (HR 2020; $V = 3.85$, $d = 16.4$ pc) was among the first main-sequence stars determined from *IRAS* observations to have a significant infrared excess caused by attendant protoplanetary material (Gillett et al. 1984). Optical images of β Pic obtained with a stellar coronagraph revealed scattered light from a circumstellar (CS) disk of dust extending 400 AU from the star and viewed nearly edge-on (Smith & Terrile 1984). Subsequent studies at infrared (Gillett 1986; Telesco, Becklin, & Wolstencroft 1988; Telesco & Knacke 1991; Backman, Gillett, & Witteborn 1992), optical (Paresce & Burrows 1987; Gledhill, Scarrott, & Wolstencroft 1991; Vidal-Madjar et al. 1992), and submillimeter wavelengths (Becklin & Zuckerman 1990; Chini et al. 1991) have resulted in widely varying conclusions regarding the size and distribution of the dust grains in the disk. Artymowicz, Burrows, & Paresce (1989) successfully reproduced *IRAS* and optical-coronagraph data using disk models which assumed a single spatial distribution of either medium (1–40 μm) or large (>40 μm) size grains. Extending the models to include ground-based infrared-flux measurements, Backman et al. (1992) were unable to reproduce both the spectral energy distribution and source dimensions of the disk with a single grain component. Instead, they found that models with two components, differing in either grain size or spatial distribution across a disk radius of 80 AU, produced adequate fits to the optical and infrared data. Specifically, the models required a region extending inward from 80 AU to 1–30 AU with a lower density and either a smaller grain size or a less-steep spatial gradient (or a combination thereof) than those deduced for the region beyond 80 AU.

Optical photometry of the β Pic disk has been reported from coronagraphic imaging of the region between 100 and 400 AU from the star (Smith & Terrile 1984; Paresce & Burrows 1987; Artymowicz et al. 1989). Although the projected widths of the occulting masks used in obtaining these images were no larger than 7″ (occulting no more of the disk than the region within 60 AU of β Pic), accurate measurement of the surface brightness of the disk within 100 AU of β Pic was prevented by mask-edge effects, saturation of the CCD analog-to-digital conversion, or the imperfect subtraction of the stellar seeing disk. The last effect is the most difficult to quantify, as even the most carefully executed control-star observation is subject to transient seeing effects and instrumental aberrations which cause differences in the scattered-light profiles of successive stellar images. The residuals from the subtraction of a slightly misshapen or misaligned control-star image can be as large as the disk brightness itself within a few arcseconds of β Pic.

In this *Letter*, we describe new CCD images of the β Pic disk obtained with the Adaptive Optics Coronagraph which expose the disk inward to a distance of 40 AU from the star. By employing a different technique for the subtraction of the stellar seeing disk, we report the first reliable disk photometry within 100 AU of β Pic. We also confirm the report by Gledhill et al. (1991) of an asymmetry between the midplane surface brightnesses of the opposing extensions of the disk beyond 250 AU.

## 2. OBSERVATIONS AND DATA REDUCTION

Observations of β Pictoris were conducted on UT 1991 December 23–24 using the 2.54 m DuPont telescope at Las Campanas Observatory and the Johns Hopkins University Adaptive Optics Coronagraph (AOC). The AOC employs an image-motion compensation system for improved resolution

[1] Based on data obtained at Las Campanas Observatory.

and pupil-plane apodization for the suppression of light diffracted by the telescope aperture (Durrance & Clampin 1989; Golimowski et al. 1992). The AOC was configured to reimage the telescope focal plane at f/45 onto a Tektronix CCD with 1024 × 1024 21 $\mu$m pixels (LCO TEK No. 2), providing a plate scale of 0.″037 pixel$^{-1}$. The CCD gain was set to 3.8$e^-$/DN, and the read noise was 8$e^-$. Circular occulting masks of projected diameters 4″ and 6″ were inserted at the reimaged focal plane preceding the CCD. These mask sizes were selected so that good signal-to-noise ratios would be obtained over the region of the disk between 40 and 400 AU without saturating the detector.

Once acquired, $\beta$ Pic was centered behind the occulting mask by finely adjusting the alignment of the image-motion compensation system with respect to the coronagraphic axis. The star's position was held fixed throughout the CCD exposure by applying image-motion corrections with a tip-tilt mirror every 10 ms. The estimated improvement in image resolution was ~0.″9 to ~0.″7, or 28% (Golimowski et al. 1992). A series of 10 exposures totaling 2450 s was recorded using the 4″ mask and an $R$ filter (2 mm OG570 + 3 mm KG3) designed to match the standard Johnson-Cousins bandpass (Bessell 1990). This series was followed by two 250 s exposures recorded with the AOC mounting base rotated 90° so that any instrumental artifacts in the processed disk image could be isolated. Two sets of two 600 s exposures were recorded using the 6″ mask which was offset to the NE and SW corners of the field. These offsets permitted maximum coverage of the disk, which is oriented at a position angle of 30°. For each mask size and location, a series of control exposures was recorded using either $\kappa$ Phoenicis (A7V, $V = 3.94$) or HR 2435 (A0II, $V = 4.39$), two stars with no known infrared excess. After each exposure series, the telescope was offset ~1′ to a region of blank sky, and an exposure of appropriate duration was recorded. Images of three photometric-standard stars were recorded each night, with attention given to zenith distance to minimize any photometric error induced by recent volcanic eruptions.

The raw CCD images were reduced to flux calibrated images using the NOAO IRAF software to perform the conventional techniques of bias subtraction, division by a flat field, interpolation over bad pixels and cosmic-ray events, and sky subtraction. Before summing the constituent images of each exposure series, each image was shifted to ensure proper alignment of the seeing disks. The alignment of two images was determined by shifting one image in increments of $\frac{1}{4}$ pixel until a minimum in the variance of the difference image was obtained. (The region of the difference image containing the misaligned occulting masks was software masked to prevent skew statistics.) After summing the aligned frames, the occulted region was replaced with an appropriately sized and centered software mask. A first attempt to subtract the seeing disk from the 4″ mask images of $\beta$ Pic followed the technique outlined by Artymowicz et al. (1989). After the control-star image was aligned with the $\beta$ Pic image in the manner described above, a radially dependent multiple of the control-star image was subtracted from the $\beta$ Pic image so that the difference was null along the line perpendicular to the midplane of the CS disk. This produced a poor result, indicating that the seeing disks of the control star and $\beta$ Pic were azimuthally discordant. A second attempt at extricating the CS disk employed both a radially and azimuthally dependent multiple of the control star, so that the difference image was null along the lines perpendicular to and at least 30° from the disk midplane. The results were much improved, but it remained evident that, within the region 4″ from $\beta$ Pic, the mismatched seeing disks produced an oversubtracted CS disk in the 10 × 245 s image and an undersubstracted CS disk in the 2 × 250 s image obtained with the AOC rotated 90°. Further, it was possible that the CS disk itself contributed to the angular dependence of the control-star scaling function. Since the resulting images were unsatisfactory and the subtraction errors unquantifiable, the technique was supplanted by one which involved self-subtraction of the $\beta$ Pic seeing disk. A synthetic seeing profile was created by fitting a 40th order Legendre polynomial to the average radial scattered-light profile obtained from image sections located at least 60° from the midplane of the CS disk. For each image pixel, the value of the synthetic profile was computed analytically and then subtracted. This technique not only produced visually superior results, but added no noise to the resultant image. The process was repeated for the control-star image using a synthetic profile created from the radial average over the entire seeing disk. The residuals of the resultant image were then used to estimate the subtraction errors in the final CS-disk image. This self-subtraction technique was successfully applied to all the reduced $\beta$ Pic and control-star images.

## 3. RESULTS

The result of the self-subtraction of the seeing disk from the 10 × 245 s image is shown in Figure 1 (Plates L7 and L8). The CS disk is clearly seen extending to the NE and SW of $\beta$ Pic beyond a radius of 40 AU. (This limit corresponds to the 2.″5 radius of the software mask and does not reflect a physical boundary of the disk.) The superposed circle of radius 6″ (~100 AU) marks the inner limit of the disk photometry reported by Smith & Terrile (1984), Paresce & Burrows (1987), and Artymowicz et al. (1989). The accompanying contour map depicts the $R$-band surface-brightness isophotes from 18 to 13 mag arcsec$^{-2}$. These contours closely resemble those shown in Figure 1 of Artymowicz et al. (1989) and reveal no obvious morphological differences between the two extensions of the disk. The FWHM of each extension perpendicular to its midplane measures 1.″9 ± 0.″2 (32 ± 3 AU) in the region 40–115 AU from $\beta$ Pic, then increases monotonically outward, measuring ~3.″7 (~60 AU) at a distance of 200 AU. (It should be noted that the NW and SE quadrants of Fig. 1 have been cleared of residual features which were confirmed artifacts of the self-subtraction process. The NE and SW quadrants, containing the midplane of the disk, have not been altered.)

For each extension of the disk, the midplane surface brightness in the region 40–450 AU from $\beta$ Pic is shown in Figure 2. The data represented at distances ≤200 AU originate from the 4″ mask image of Figure 1, while beyond 200 AU the data are taken from the higher signal-to-noise 6″ mask images. (The 6″ mask data were offset by −0.39 and −0.06 mag arcsec$^{-2}$ in the NE and SW extensions, respectively, in order to match the 4″-mask data at 200 AU.) The error bars for the data reflect the following, combined in quadrature: (1) statistical errors from photon noise and pixel arithmetic, (2) the rms of the residuals from the self-subtraction of the seeing disk in the corresponding control-star image (normalized to the brightness of $\beta$ Pic), and (3) the rms deviation of the disk brightness due to a possible $\frac{1}{4}$ pixel misalignment of the centers of the fitted seeing profile and the actual seeing disk. As expected, the errors within 100 AU were dominated by the subtraction of the seeing

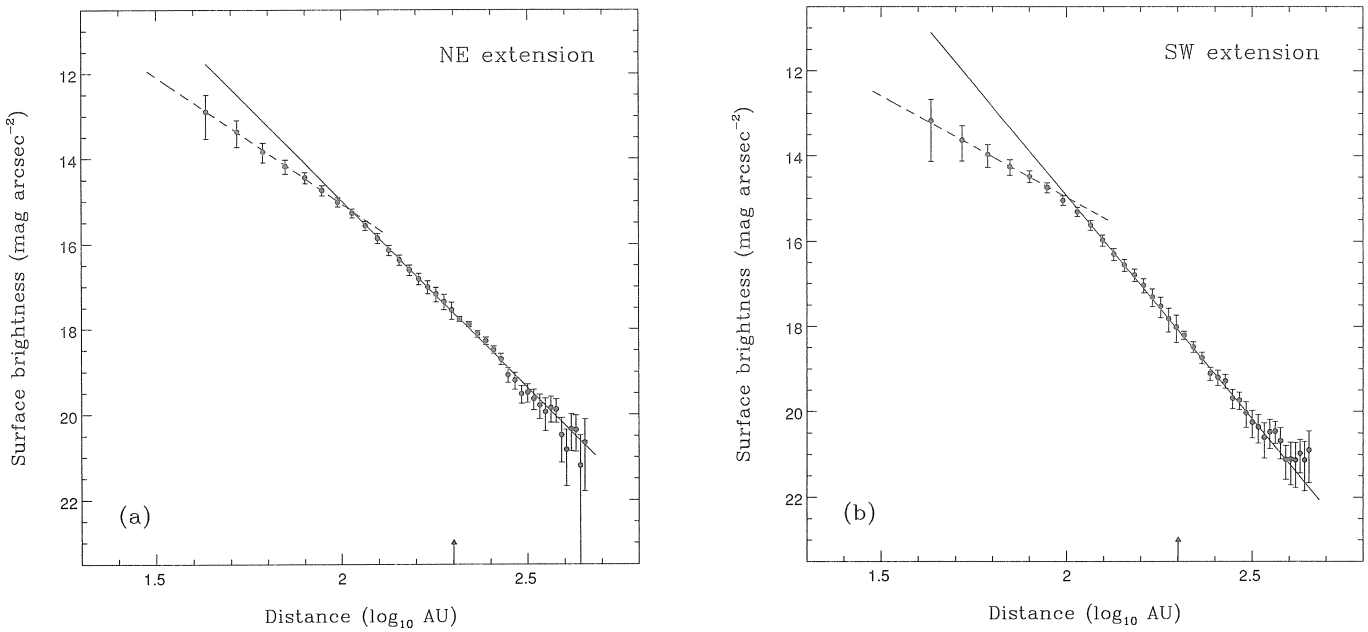


FIG. 2.—(*a*) The midplane surface brightness of the NE extension of the β Pic disk. The arrow at 200 AU marks the point where the data from the 4″ and 6″ mask images are combined. The slopes of the dashed and solid lines are −2.4 and −3.5, respectively, and represent the indices of the radial power laws which best fit the data in the regions 40–90 AU and 100–300 AU from β Pic. (*b*) The same as (*a*) but for the SW extension. The slopes of the dashed and solid lines are −1.9 and −4.2, respectively.

disk, while those beyond 300 AU were dominated by photon noise. At 100 AU, the midplane surface brightness of each extension is 15.0 mag arcsec$^{-2}$, which is nearly 1 mag arcsec$^{-2}$ brighter than that reported by Smith & Terrile (1984) and Paresce & Burrows (1987). This result is independent of the technique chosen for subtraction of the seeing disk. (Differences in the disk brightness resulting from the various techniques are significant only for the data within ∼60 AU. The data depicted in Figure 2 for this region lie between those obtained from the oversubtracted and undersubtracted cases described in § 2, as expected). Since the disk is resolved in their images as well as in ours, the reason for this discrepancy (barring a systematic error in photometry) is unclear.

Two characteristics of the data displayed in Figure 2 are immediately striking: (1) an abrupt change in the gradient of the midplane surface brightness of the disk across 100 AU, and (2) an asymmetry between the brightness gradients of the two extensions of the disk. For each extension, the radial dependences of the surface brightness within the regions 40–90 AU and 100–300 AU are well-fitted by power laws, $I \propto r^{\nu}$, with the following indices:

$$\text{NE extension:}\quad \nu_{r<90\,\text{AU}} = -2.38^{+0.79}_{-0.65}\,,$$
$$\nu_{r>100\,\text{AU}} = -3.508 \pm 0.003\,;$$
$$\text{SW extension:}\quad \nu_{r<90\,\text{AU}} = -1.91^{+0.95}_{-0.82}\,,$$
$$\nu_{r>100\,\text{AU}} = -4.182 \pm 0.004\,.$$

These indices are the slopes of the lines shown in Figure 2 which best fit the data within each region. (Because the error bars shown in Figure 2 do not represent the convolution of purely random errors, the uncertainties ascribed to the power-law indices deserve explanation. The indices themselves are obtained from the data and their associated photon noise, the latter being the only truly statistical weights of the data. The uncertainties given above reflect the range of indices [i.e., slopes] accommodated by the error bars of the data lying within the respective regions of the disk. When no such range satisfied these constraints, the uncertainty of the index was determined from the least-squares fit to the data.) The indices for the regions 100–300 AU from β Pic are ∼10% smaller than those obtained by Gledhill et al. (1991) for the regions between 250 and 500 AU, but show that the asymmetric surface brightness is not restricted to the outer regions of the disk. Curiously, Smith & Terrile (1984) and Artymowicz et al. (1989) quote indices of −4.3 and −3.6, respectively, for *both* extensions of the disk. Our results also suggest that the sense of the asymmetry inverts across 100 AU, as noted by Vidal-Madjar et al. (1992) on morphological grounds, but the uncertainties attached to the indices for $r < 90$ AU accommodate either sense, including no asymmetry at all.

As the seeing disk of the control star was found to be less azimuthally symmetric than that of β Pic in the 4″-mask images, the uncertainties of the data within than 100 AU are probably overestimates. Despite this conservative error assessment, the surface brightnesses in this region of the disk measure 2–10 σ below those projected from the power-law fit beyond 100 AU. That this rather abrupt change in brightness gradient occurs exactly at the inner limit of previously published disk photometry is perhaps not coincidental. Artymowicz et al. (1989) alluded to a possible departure from the power law at ∼100 AU, but could not specify whether the effect was real or an artifact of the control-star subtraction. In a subsequent paper, Artymowicz, Paresce, & Burrows (1990) indicated a change in the power-law index at ∼100 AU from −4 to −3, but provided no estimate of their subtraction errors.

## 4. DISCUSSION

Our observations reveal a distinct change in the nature of the $\beta$ Pic disk occurring across a radius of 100 AU. The abrupt flattening of the brightness gradient at 100 AU suggests either a sudden change in the scattering properties of the grains (caused by a smaller grain size or changing albedo), a decrease in the number density of the grains, or both. Although the first possibility cannot be investigated with $R$-band photometry alone, it can be checked by comparing the results of multicolor imaging of the disk. Vidal-Madjar et al. (1992) have reported noncoronagraphic observations of the disk 30–200 AU from $\beta$ Pic with an antiblooming CCD and standard $BVRI$ filters. They found that the midplane surface brightness followed an $r^{-3.6}$ power law over the observed region in all bandpasses except $B$. In blue light, the disk brightness departed from the power law at radii $\lesssim$75 AU, becoming a factor of 4 times underluminous at 30 AU. They concluded that a change in the albedo and not in the size of the grains could account for these results. It is surprising that Vidal-Madjar et al. (1992) did not detect a departure from the power law in their $R$-band images as well, since our images indicate brightness deficiencies within 100 AU comparable to their $B$-band measurements. It is possible that their results suffer from the effects of poorer seeing conditions (1″–2″), an unapodized telescope pupil, or CCD read noise (which may dominate the disk brightness for exposures as brief as 0.5 s). Additional multicolor observations are clearly needed to resolve this discrepancy.

A change in the brightness gradient resulting from a decreased number density is consistent with the notion of a two-component disk introduced by Backman et al. (1992) in their models of the spatial and spectral energy distributions of the disk. In these models, an outer component of the disk was defined according to the results of previous optical-bandpass observations. Specifically, the radial power-law index $\gamma$ of the optical thickness perpendicular to the disk midplane (i.e., the spatial gradient of the vertical optical depth) was fixed at $-1.7$ for the outer component, in accordance with the best-fit model of Artymowicz et al. (1989). The grain size and $\gamma$ for a hypothetical inner component were varied independently until the parameter space of reasonable fits to the measured infrared fluxes and source sizes was delimited. For those models in which $\gamma$ was varied, good fits were obtained when the spatial gradient of the inner component was less steep than that of the outer component ($\gamma \sim -0.5$ versus $-1.7$). This result implies that the vertical thickness of the disk increases with radius in the outer component, whereas a flatter spatial distribution exists in the inner component. This scenario is consistent with our measurements of the FWHM of the disk which show a nearly constant thickness within $\sim$115 AU and an increasing thickness beyond $\sim$115 AU. Although Backman et al. (1992) fixed the boundary between the two disk components at 80 AU (as a compromise among the best fits to individual measurements), they found that the best fit to the overall spectral energy distribution was achieved with a boundary of 100 AU. Additional modeling is needed to determine whether the observed brightness gradients within 100 AU are sufficiently flat to be consistent with both the measured vertical thickness and the results obtained by Backman et al. (1992) for the vertical optical depth of the inner component. However, if we crudely apply the relation $\nu = \gamma - 2$, which is relevant in the region beyond 100 AU (Nakano 1990; Backman et al. 1992), we obtain $\gamma = -0.38$ and $+0.09$ for the NE and SW extensions, respectively. Both results are compatible with the desired $\gamma \sim -0.5$ for the inner component.

The changes in the disk characteristics noted at $\sim$100 AU from $\beta$ Pic must reflect changing thermodynamic or kinetic processes in that region of the disk. Nakano (1988) predicted a discontinuity in the grain composition at a radius coinciding with a disk temperature of 100 K, which marks the limit of rapid sublimation of small icy grains. Although the location of this limit depends on the assumptions made for the characteristic grain size, Backman et al. (1992) determined from their models that the sublimation limit is nearly coincident with the boundary between the two disk components. Thus, the outer component is likely to be dominated by high-albedo icy grains, whereas the inner component consists primarily of refractory grains. The detection of 10 $\mu$m emission from silicates within 50 AU (Telesco & Knacke 1991) supports this scenario. Several authors have also suggested the presence of an innermost void of outer radius 1–30 AU, sustained perhaps by planetary accretion (e.g., Smith & Terrile 1984; Telesco et al. 1988; Artymowicz et al. 1989; Backman et al. 1992). The flattened brightness gradient and the uniform disk thickness observed within $\sim$100 AU may therefore reflect a transition between the outer region of grains in orbits inclined at $\lesssim 10°$ and an innermost region of planetesimals in nearly coplanar orbits.

The authors thank the Seaver Insitute and the Center for Astrophysical Sciences at Johns Hopkins University for their support of the Adaptive Optics Coronagraph project. We gratefully acknowledge The Observatories of the Carnegie Institution of Washington for providing observing time at Las Campanas, as well as the observatory staff for their dedicated assistance. Finally, we thank D. Backman for his comments on the manuscript.

## REFERENCES

Artymowicz, P., Burrows, C., & Paresce, F. 1989, ApJ, 337, 494
Artymowicz, P., Paresce, F., & Burrows, C. 1990, Adv. Space Res., 10 (3), 81
Backman, D. E., Gillett, F. C., & Witteborn, F. C. 1992, ApJ, 385, 670
Becklin, E. E., & Zuckerman, B. 1990, in Submillimetre Astronomy, ed. G. D. Watt & A S. Webster (Dordrecht: Kluwer), 147
Bessell, M. S. 1990, PASP, 102, 1181
Chini, R., Krügel, E., Shustov, B., Tutukov, A., & Kreysa, E. 1991, A&A, 252, 220
Durrance, S. T., & Clampin, M. 1989, Proc. SPIE, 1114, 97
Gillett, F. C. 1986, in Light on Dark Matter, ed. F. P. Israel (Dordrecht: Reidel), 61
Gillett, F. C., Aumann, H. H., Low, F. J., Neugebauer, G., & Waters, R. 1984, paper presented at Protostars and Planets II Conf. (Tucson)
Gledhill, T. M., Scarrott, S. M., & Wolstencroft, R. D. 1991, MNRAS, 252, 50P
Golimowski, D. A., Clampin, M., Durrance, S. T., & Barkhouser, R. H. 1992, Appl. Opt., 31, 4405
Nakano, T. 1988, MNRAS, 230, 551
———. 1990, ApJ, 355, L43
Paresce, F., & Burrows, C. 1987, ApJ, 319, L23
Smith, B. A., & Terrile, R. J. 1984, Science, 226, 1421
Telesco, C. M., Becklin, E. E., Wolstencroft, R. D., & Decher, R. 1988, Nature, 335, 51
Telesco, C. M., & Knacke, R. F. 1991, ApJ, 372, L29
Vidal-Madjar, A., et al. 1992, Messenger, 69, 45

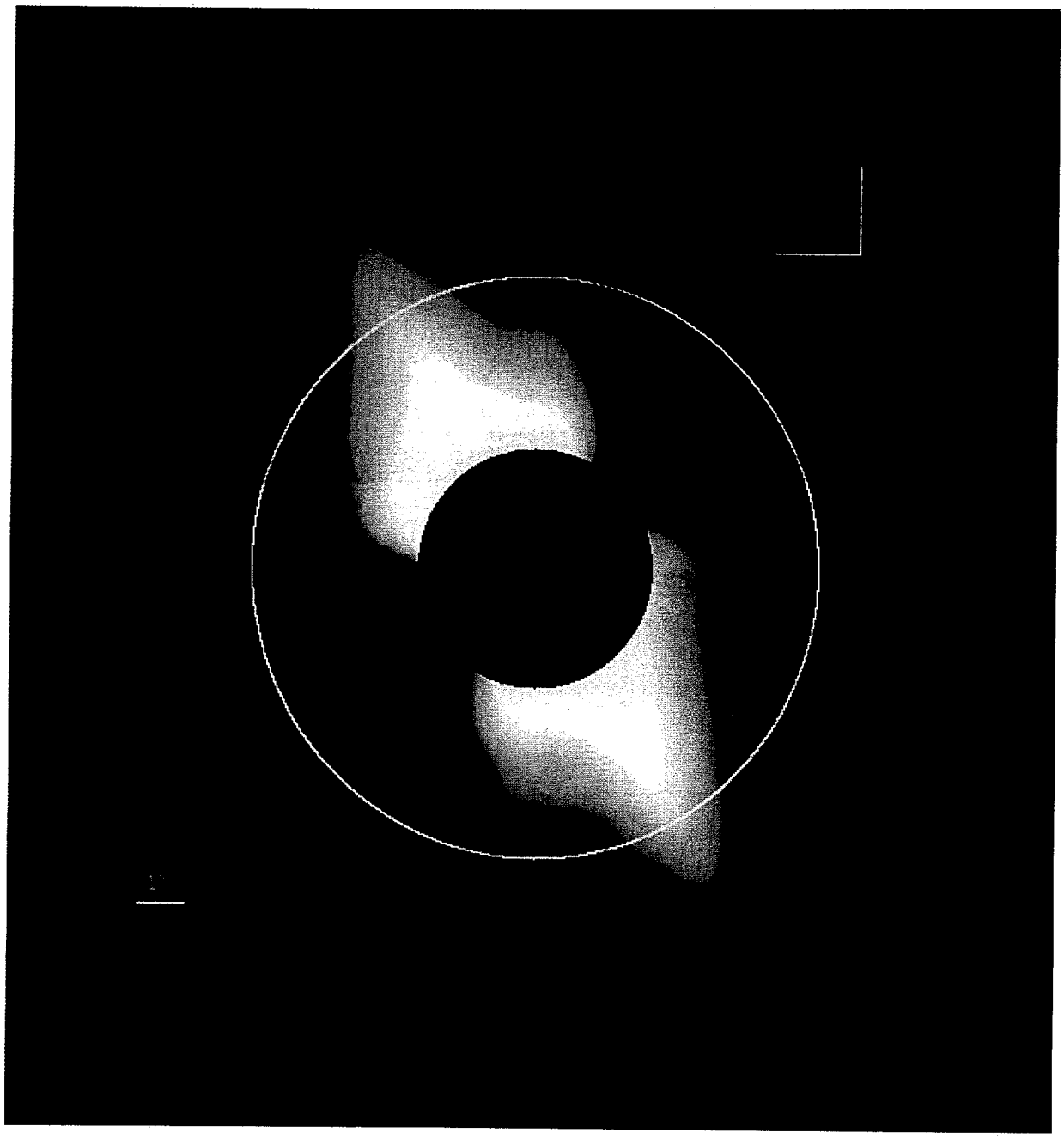

FIG. 1*a*

FIG. 1.—(*a*) *R*-band image of the $\beta$ Pictoris circumstellar disk obtained with the Adaptive Optics Coronagraph. The field is 22.″5 × 24″, and the radius of the occulted region is 2.″5 (40 AU). The superposed circle of radius 6″ (100 AU) marks both the location of the change in the midplane brightness gradient and the limit of previously published disk photometry. The scattered light from $\beta$ Pic has been removed by azimuthally subtracting a synthetic seeing profile which best fit the stellar seeing disk. The NW and SE quadrants of the image have been cleared of features which were confirmed artifacts of the subtraction process. (*b*) Contour map of the *R*-band image. The contours reflect the surface brightness isophotes from 18 to 13 mag arcsec$^{-2}$ at intervals of 0.5 mag arcsec$^{-2}$.

GOLIMOWSKI, DURRANCE, & CLAMPIN (see 411, L42)

PLATE L8

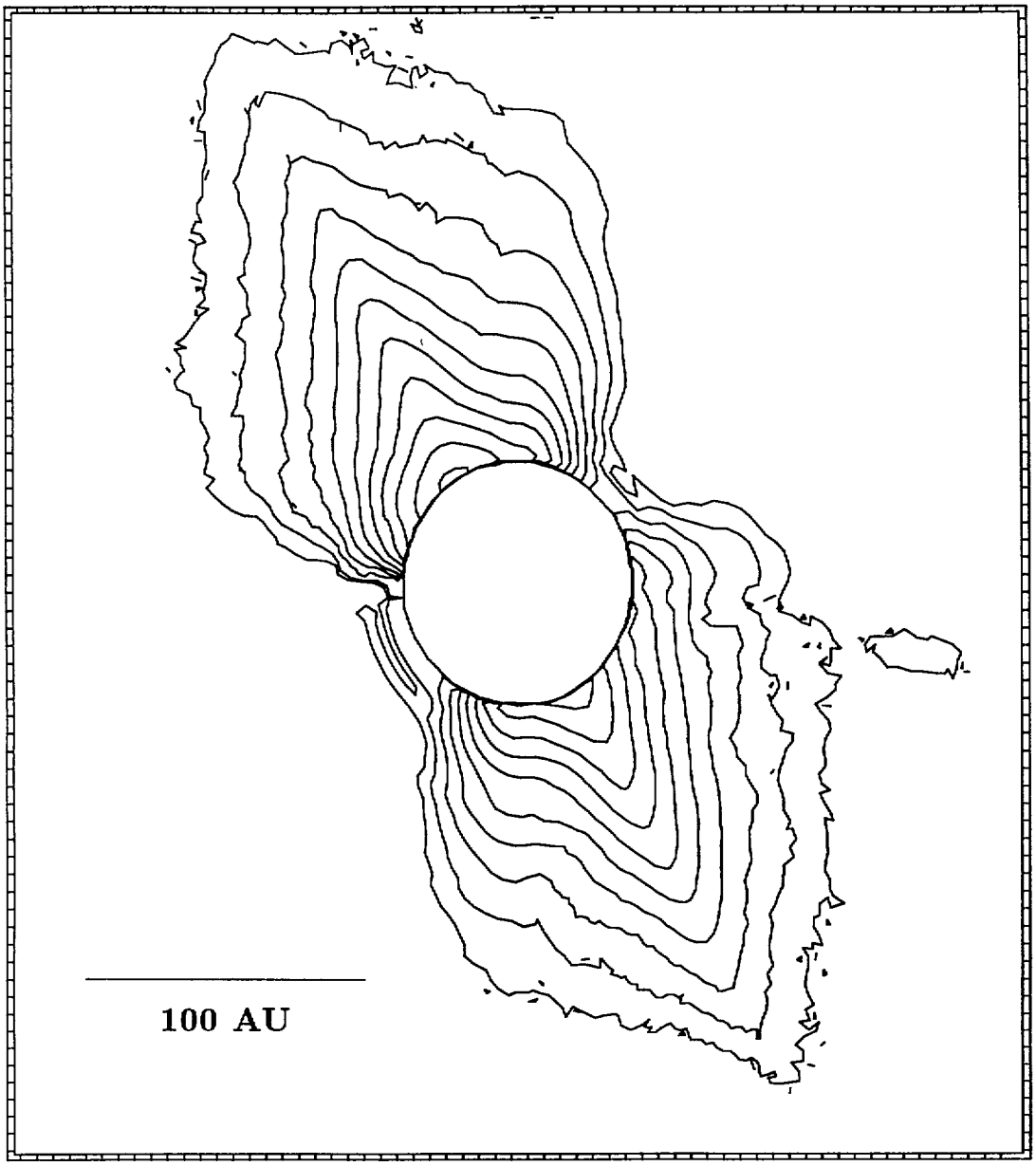


FIG. 1*b*

GOLIMOWSKI, DURRANCE, & CLAMPIN (see 411, L42)